



Hierarchical nested-network porous copper fabricated by one-step dealloying for glucose sensing



Xuequan Li, Baisheng Huang, Cuicui Qiu, Zhou Li, Li-Hua Shao^{*}, Hong Liu^{**}

Beijing Institute of Nanoenergy and Nanosystems, Chinese Academy of Sciences, National Center for Nanoscience and Technology (NCNST), Beijing, 100083, PR China

ARTICLE INFO

Article history:

Received 6 February 2016

Received in revised form

19 April 2016

Accepted 21 April 2016

Available online 22 April 2016

Keywords:

Hierarchical nested-network

Porous copper

Dealloying

ABSTRACT

A novel freestanding hierarchical nested-network porous copper (HNNPC) was fabricated by one-step free dealloying. The $\text{Al}_{75}\text{Cu}_{25}$ (at.%) alloy precursor was prepared with both pure Al phase and the intermetallic Al_2Cu phase. The microstructure of the alloy led to the hierarchical porous structure characterized by larger ligaments (pores) at micron scale (ca. 3–5 μm) and the smaller ligaments (pores) at nanoscale (ca. 50–60 nm) through dealloying. The morphology, crystal structure, elemental analysis, surface area, pore sizes distribution, electrochemical and sensing properties of HNNPC have been studied. The resulted HNNPC had bicontinuous hierarchical structure, which met the electrochemical or chemical applications' requirements, namely, (1) the larger pores providing rapid transport pathways for fast switching and (2) smaller pores at nanoscale having the large surface area for functionalization. The CV and EIS of HNNPC presented an electro-catalytic activity to glucose, which was promising as a glucose sensor with excellent sensitivity. Furthermore, HNNPC itself could also be a host of other active materials.

© 2016 Elsevier B.V. All rights reserved.

1. Introduction

Hierarchical porous materials represent a class of functional materials for numerous applications due to their hierarchy of porosities and structure sizes. They can act as self-contained units, and also can host materials to incorporate other active components to realize catalysis, sensing, energy storage and other applications [1–7]. Hierarchical porous metal is a significant subset of hierarchical porous materials, which is promising for various applications due to their superior electrical, optical and mechanical properties [8]. Especially for the electrochemically or chemically driven devices, the hierarchical structure of porous metals exactly meet the application requirements, namely, (1) the larger pores providing rapid transport pathways for fast switching and (2) smaller pores at nanoscale having the large surface area for functionalization. Therefore, intense attentions have been paid to fabricate hierarchical porous metals on account of the enormous potential applications [9,10]. Dealloying, the selective dissolution of the less noble component from an alloy [11], plays a vital role in fabricating the hierarchical porous metals. The hierarchical porous gold has been

obtained by dealloying the deposited gold and silver alloy on the bijels template with several steps [10]. A two dealloying steps method has also been used to synthesize the nested-network nanoporous gold [12–14]. However, the barriers such as high cost, complicated fabrication process and limited structure size restrict the applications of gold.

Copper and its oxides as the stable and cost-effective materials have attracted intensive attentions. A range of exquisite nanostructures such as hollow nanopowders [15] Nanorods [16], nanocubes [17,18], nanowires [19], nanoparticles [20,21], nanopores [22] and so on, have been synthesized for the reason of larger active surface areas and better catalytic properties compared to the bulk materials. Several routes have been proposed to fabricate the hierarchical porous copper [23–25]. However, the resulted structure and also the electrochemical properties are not satisfied. Up to now, it is still a big challenge to fabricate hierarchical porous copper with the structure sizes at both micron and nano scales by means of a cost-effective simple method.

Here, a novel strategy was used to generate hierarchical nested-network porous copper (HNNPC) that consisted of micron-porous and nanoporous bicontinuous structures. The copper and aluminum alloy with intermetallic phase Al_2Cu was obtained by melting in a horizontal tube furnace and cooled down slowly afterwards. The HNNPC was fabricated by chemical dealloying in 1 M

^{*} Corresponding author.

^{**} Corresponding author.

E-mail addresses: shaolihua@buaa.edu.cn (L.-H. Shao), hliu@binn.cas.cn (H. Liu).

HCl aqueous solution at 50 degree centigrade under vacuum. The electrochemical performance of HNNPC was measured showing an electro-catalytic activity to glucose, which is promising used as a glucose sensor. Furthermore, HNNPC itself is also a good host of other active materials.

2. Experimental

2.1. Sample preparation

Master alloy Al₇₅Cu₂₅ (at.%) was melted in a horizontal tube furnace (Beiyike, BTF-1200C-PV, China) from Cu (99.99%) and Al (99.99%) at 800 °C under argon atmosphere for 24 h at a ramp rate of 5 °C min⁻¹, then cooled down at 2 °C min⁻¹ to room temperature. The as-prepared alloy ingot was cut into cuboids with the dimension of 1 mm × 5 mm × 10 mm by a wire saw (Shenyang Kejing Instrument Co., LTD, STX-202A, China). The chemical dealloying was taken in 1 M HCl aqueous solution at 50 °C in vacuum.

2.2. Electrochemical test

The sample electrode was immersed in the solution totally during electrochemical measurement with a macroscopic size 1 mm × 5 mm × 10 mm. The effective area, *S*, was calculated by the equation, $S = A \times m$, where *A* is the specific surface area and *m* is the mass of the electrode. Cyclic voltammetry (CV) and electrochemical impedance spectroscopy (EIS) measurement were performed in a standard three electrodes system in 0.25 M NaOH aqueous solution with a potentiostat (Autolab, PGSTAT100N, Switzerland). The Ag/AgCl (in 3 M KCl solution, Autolab, Switzerland) was used as reference electrode, the platinum plate was counter electrode and the sample was working electrode. The potential window for CV was set in the range from -1.3 V to 0.8 V. The impedance measurement carried out with frequency from 0.1 Hz to 100 kHz.

2.3. Materials characterization

Cold-field emission scanning electron microscope (SEM, HITACHI SU8200, Japan) equipped with energy dispersive spectrometer (EDS, IXRF, USA) was used to characterize the microstructures and phase distribution of the HNNPC. X-ray diffraction (XRD, MXP21VAHF, MAC Science Co., Ltd., Japan) was carried out with a Cu-K α radiation source. Micromeritics surface area and porosity analyzer (ASAP 2020 HD88, USA) was used to analyze the total surface area through nitrogen sorption. The degas process was carried out at 250 °C for 4 h under a vacuum of 500 μ m Hg (~0.67 mbar). Liquid nitrogen was employed to maintain the temperature throughout adsorption-desorption process. The nanopores surface area and pore diameter were analyzed by Barrett-Joyner-Halenda (BJH) method. The t-method was applied to calculate the pore volume of the nanopores and the specific surface area.

3. Results and discussion

3.1. Phase constitution of the as-prepared alloy

Fig. 1(a) shows the SEM image of the as-cast Al₇₅Cu₂₅ alloy constituent distribution consisting of two distinct phases. They are pure Al phase (the dark part) and intermetallic phase Al₂Cu (the light part), which can also be confirmed by XRD (Fig. 3(a)). In order to verify the distribution of the two phases in the casted alloy, EDS mapping was performed. It is obvious that the element Al and Cu distinguish each other by the overlay mapping of the two elements,

as shown Fig. 1(b). To illustrate the distribution of the two elements more clearly, the individual element mapping was crucial. As shown Fig. 1(c), the element Al exists in both the light part and the dark part, which is not observed in the overlay mapping due to the signal of element Cu being much stronger than that of the element Al in the light part. In contrast, the element Cu (Fig. 1 (d)) only exists in the light part. Therefore, the light part is the intermetallic phase Al₂Cu, and the dark part is the pure Al phase.

The AlCu alloy here with approximate pure Al phase plus the intermetallic Al₂Cu phase obtained by melting and slow cooling in a horizontal tube furnace differs with the previous reported ones in the literatures [26–29]. The Al₇₅Cu₂₅ alloy cast by arc melting has been found the existence of both the pre-eutectic Al₂Cu phase and the lamellar eutectic α -Al/Al₂Cu phase [30]. But the lamellar eutectic α -Al/Al₂Cu phase is not profitable to develop bicontinuous porous structures due to its lamellar structure. The lamellar eutectic α -Al/Al₂Cu phase can be eliminated by annealing, which gives rise to much coarser α -Al phase than the original one and increased the size of eutectic Al₂Cu phase. Both of them hinders the evolution of the hierarchical porous microstructures. Contrarily, the as-prepared AlCu alloy in this work was melted in a horizontal tube furnace for a long time including the well-defined approximate pure Al phase and Al₂Cu phase at several micron scale, respectively. According to the AlCu alloy phase diagram, the Al₇₅Cu₂₅ alloy cooling down from liquid to form an alloy followed two stages: (1) when the temperature reached the liquid line, Al₂Cu phase precipitated from the liquid phase, and more Al₂Cu phase formed with the temperature decreasing; (2) when the temperature reached the eutectic temperature, Al/Al₂Cu eutectic phase started forming until all the liquid phase solidified. In contrast, the solidification was too fast to form separated Al₂Cu phase and pure Al phase by arc melting in the literature, which led to the final constituents consisting of Al₂Cu phase and Al/Al₂Cu phase with lamellar eutectic phase [30]. Meanwhile, the fast solidification also gave rise to the nonuniform distribution of Al₂Cu phase and Al/Al₂Cu eutectic phase. Conversely, the present approach provided enough time for the solidification to involve Al₂Cu phase and approximate pure Al phase by temperature decreasing gradually in the horizontal tube furnace. Please note that to control the microstructure of the initial alloy would decide the resulted structure of the porous copper.

3.2. Microstructures of the HNNPC

Fig. 2(a) displays the overview SEM image of the HNNPC microstructures. Fig. 2(b) shows the identified bicontinuous channels with several microns. This structure has not been reported, which can be obtained by simple free dealloying. The as-produced bicontinuous larger size channels are significant for fast mass transport. It is believed that the larger pores in hierarchical porous copper are inherited from the approximate pure Al phase in the initial alloy. Meanwhile, the bicontinuous nanoporosity with smaller size at nanoscale was also produced both at the surface (Fig. 2(c)) and the cross-section of the larger ligaments (Fig. 2(d)). It is believed that they are inherited from the Al₂Cu phase in the initial alloy. Compared to bulk metal, the bicontinuous nanoporosity contributes to the large specific surface area which is significant for various applications in catalysis and sensing.

3.3. Elemental constitution of the samples

Both the development of nanopores and the hierarchical porosity are strongly affected by the Al content of the as-prepared alloy. In other words, the larger ligaments (pores) at micron scale formed from the pure Al phase and the smaller ligaments (pores) at nanoscale from the intermetallic Al₂Cu phase by dealloying. Nearly

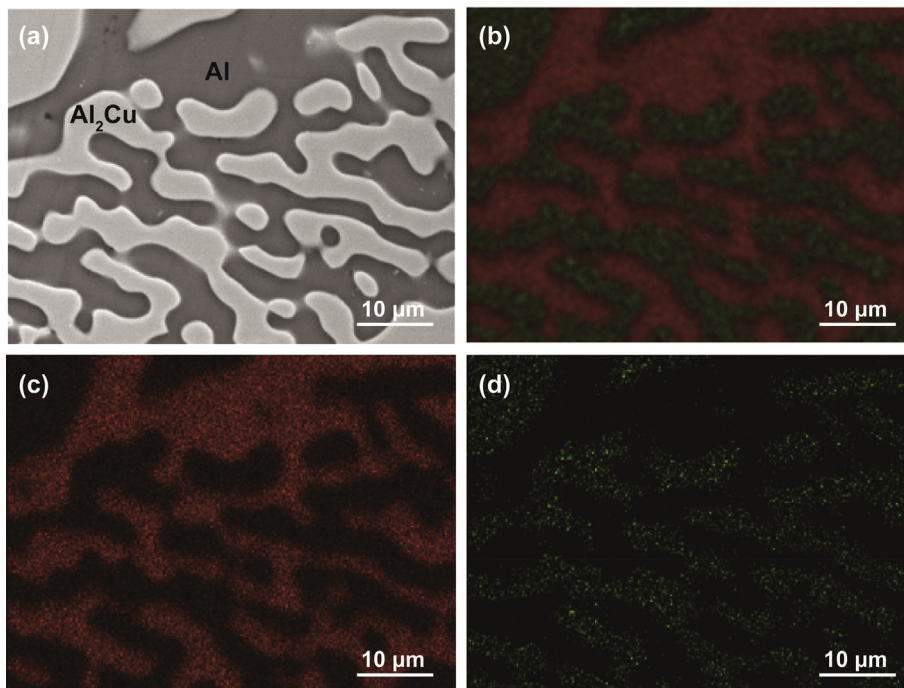


Fig. 1. (a) SEM image of the as-cast $\text{Al}_{75}\text{Cu}_{25}$ alloy consisting of approximate pure Al phase and eutectic Al_2Cu phase; Energy dispersive spectroscopy (EDS) of (b) copper and aluminum elements overlay mapping, (c) aluminum element mapping and (d) copper element mapping.

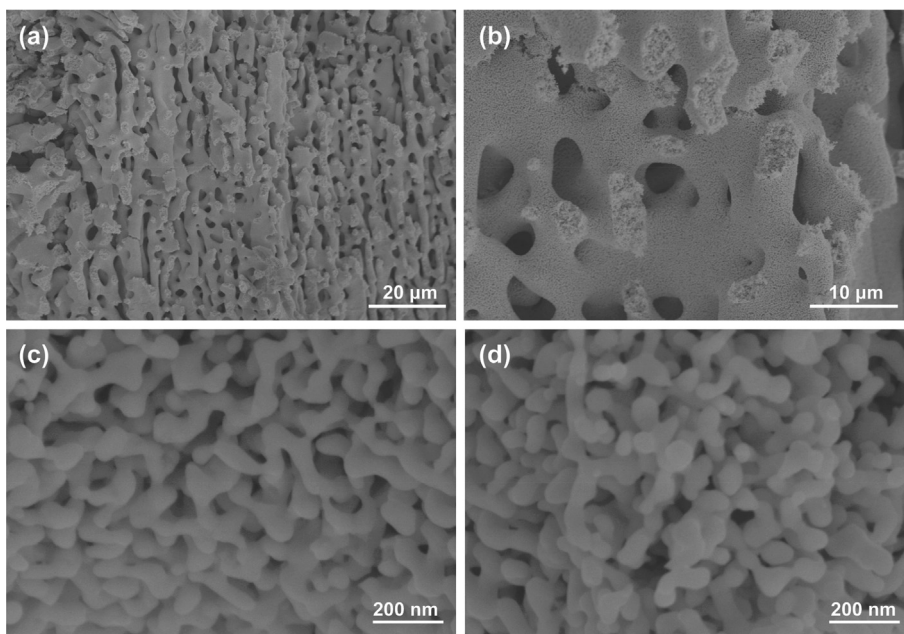


Fig. 2. SEM images of the as-prepared hierarchical nested-network porous copper: (a) The overview SEM image showing the microstructure of hierarchical porous copper; (b) higher-level porous channels and ligaments at micron scale; the nanoporous structure at the (c) surface and (d) the cross-section of the larger ligaments.

all of Al element was removed from interior of AlCu alloy after dealloying, which can be verified by XRD and EDS analysis performed on cross-section of the sample. The distinct signals of Al were observed before dealloying (Fig. 3(a) and (b)). Contrarily, only typical Cu signals can be clearly identified after dealloying as shown in Fig. 3(c) and (d).

3.4. Surface area and pore distribution of HNNPC

The specific surface area plays a critical role in various applications for porous materials. The specific surface areas were up to $47.6 \text{ m}^2 \text{ g}^{-1}$ with combination microporous areas of $22.1 \text{ m}^2 \text{ g}^{-1}$ calculated by t-method and mesoporous areas of $25.5 \text{ m}^2 \text{ g}^{-1}$ analyzed by BJH method. The effective area of the electrode was calculated by the equation

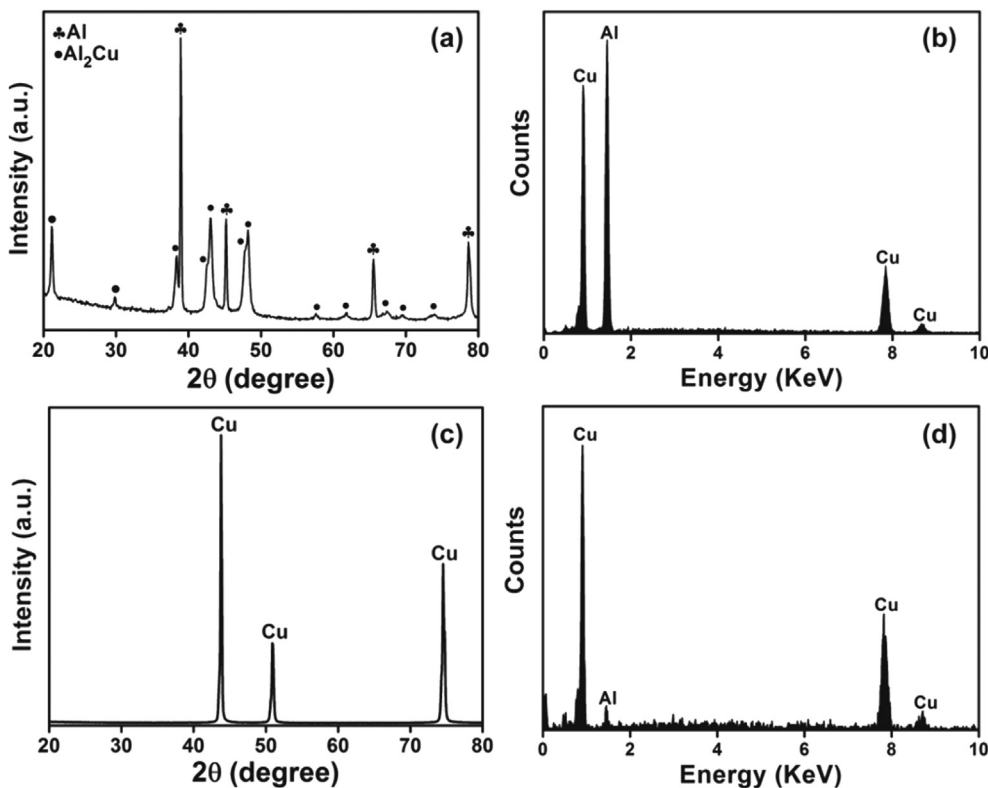


Fig. 3. XRD patterns and EDS spectra of the samples of: (a) and (b) XRD patterns and EDS spectra of the as-cast $\text{Al}_{75}\text{Cu}_{25}$ alloy; (c) and (d) XRD patterns and EDS spectra of the hierarchical nested-network porous copper.

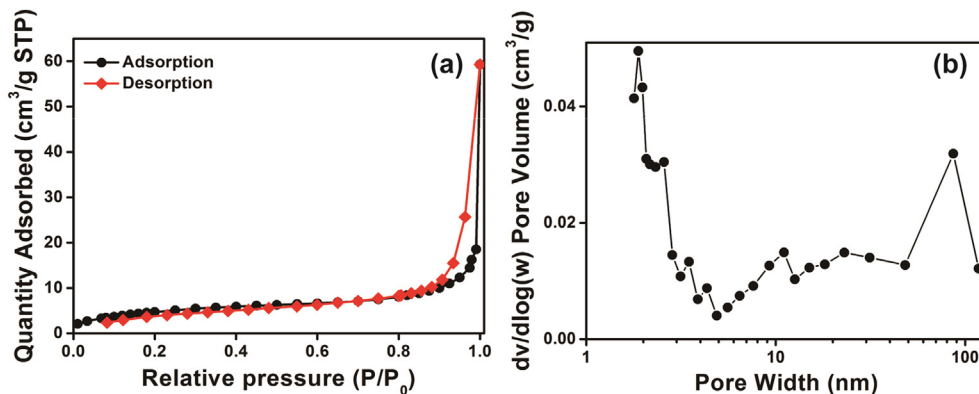


Fig. 4. (a) Nitrogen adsorption/desorption isotherms of the hierarchical nested-network porous copper; (b) pore size distribution.

$S = A \times m = 47.6 \text{ m}^2 \text{ g}^{-1} \times 0.0877 \text{ g} = 4.17 \text{ m}^2$ Fig. 4(a) displays a typical N_2 adsorption/desorption isotherms of as-prepared hierarchical nested-network porous copper. As illustrated in Fig. 4(a), the type-V nitrogen sorption isotherms with the hysteresis loop for the sample indicates the existence of mesoporous structures. Meanwhile, the hysteresis loop from 0.9 (P/P_0) to 1.0 (P/P_0) implies various pores distribution, which can be confirmed by the BJH model. The calculated distribution of pores sizes are with micropores (<2 nm), mesopores (2–50 nm) and macropores (>50 nm) as shown in Fig. 4(b). The mesopores and macropores can also be observed by SEM image.

Up to now, HNNCP was confirmed definitely with larger ligaments at micron scale, and also smaller ligaments at nanoscale forming on the larger ligaments. The idea of fabricating hierarchical

porous copper by taking advantage of intermetallic phase has been proposed, however, this HNNPC with a self-similar structure at two different length scales is similar with that of hierarchical porous gold [12–14].

3.5. Electrochemical characterization of HNNPC

Fig. 5 shows the cyclic voltammogram (CV) of the HNNPC electrode in 0.25 M NaOH aqueous solution without and with 50 mM glucose. The CV in the solution without glucose contains three oxidation peaks from -0.5 V to 0.5 V, which agrees with the results reported in literatures [31,32]. The oxidation processes are described as following [31,32]:

Oxidation peak 1 (O_1):

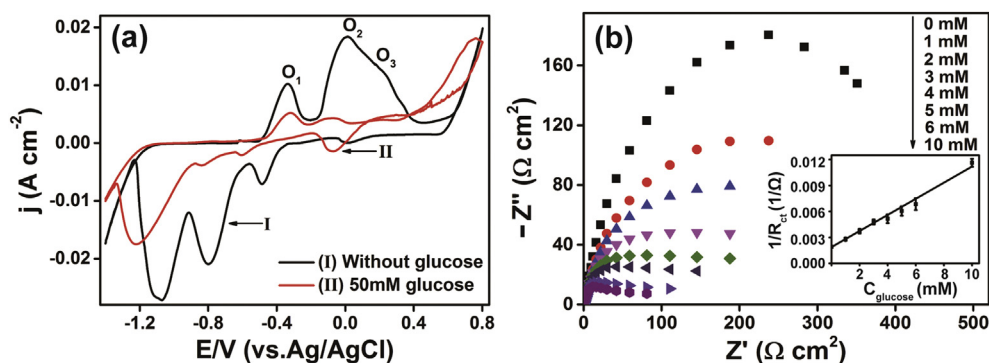
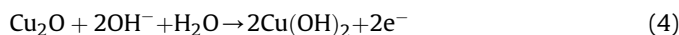


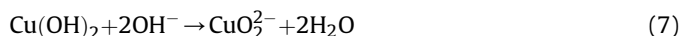
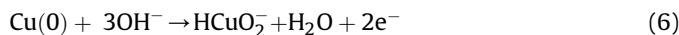
Fig. 5. (a) Cyclic voltammograms of the hierarchical nested-network porous copper with and without glucose in the 0.25 M sodium hydroxide with scan rate of 1 mV s^{-1} ; (b) The electrochemical EIS changes for the hierarchical nested-network porous copper with different glucose concentrations. Inset in (b) is the corresponding calibration curve of glucose determination.



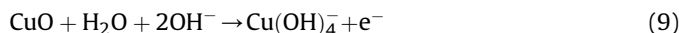
Oxidation peak 2 (O_2):



Oxidation peak 3 (O_3):



It is worth noting that $\text{Cu}(\text{OH})_2$ can be oxidized to CuOOH or $\text{Cu}(\text{OH})_4^-$ from 0.50 V to 0.60 V as the following equations shown [31,32]:



The corresponding peaks, however, cannot be observed here. And the strongly oxidizing Cu(III) species play significant role in copper electrode's electrocatalytic behavior [33,34]. With 50 mM glucose added, an obvious oxidation current was observed at 0.50 V, indicating good performance of the HNNPC towards glucose electrocatalytic oxidation. Glucose is oxidized to gluconolactone, which finally hydrolyses to gluconic acid [35–37].

The concentrations of glucose were detected using HNNPC electrode by the electrochemical impedance spectroscopy (EIS) approach. All of the EIS were measured with various concentrations of glucose and the spectra were fitted with equivalent circuit model with complex nonlinear least square approximation method. In this model, the electron transfer kinetics is illustrated by solution resistance (R_s), double layer capacitance (C_{dl}) and charge transfer resistance (R_{ct}). The equivalent circuit model and the relative parameters are summarized in Table 1.

With glucose's concentration increasing, the pores' surfaces of HNNPC electrode were covered by glucose, giving rise to more oxidized glucose and more transferred charge. Furthermore, the smaller R_{ct} implies faster charge transfer rate. Reactant increasing will increase the electrochemical reaction rate. Therefore, the

Table 1

The equivalent circuit and the values of relative parameters.

	R_{ct} (Ω)	R_s (Ω)	CPE_{dl}	N
0 mM	521	1.91	10.31	0.993
1 mM	358	1.78	9.13	0.991
2 mM	269	1.64	8.37	0.992
3 mM	209	1.36	8.26	0.993
4 mM	194	1.63	7.73	0.994
5 mM	165	1.93	6.67	0.993
6 mM	140	2.07	5.88	0.992
10 mM	86	1.66	5.04	0.993

diameter of semicircles, which stands for the R_{ct} value decreased due to the impedance decreasing with the glucose's addition. In general, all of the R_{ct} values here are much smaller than that in the literatures [38,39] due to the high specific surface area and excellent electrical conductivity of HNNPC. The relation between $1/R_{ct}$ and the glucose concentration is illustrated by $1/R_{ct} = K C_{glucose}$, in which K is a constant parameter [39]. And $1/R_{ct}$ vs. glucose concentration was plotted and the calibration curve was shown in the inset of Fig. 5(b). It showed a linear dependence of $1/R_{ct}$ on the glucose' concentration in the range of 1–10 mM with a regression coefficient of 0.992, and the corresponding fitted equation was showed below:

$$1/R_{ct} = 1.88 \times 10^{-3} + 9.3 \times 10^{-4} C_{glucose}$$

From the above equation, one can see that HNNPC is suitable for glucose concentration determination due to its excellent sensitivity.

4. Conclusions

The hierarchical nested-network porous copper (HNNPC) was fabricated by simple one-step free dealloying, which takes advantage of intermetallic phase in $\text{Al}_{75}\text{Cu}_{25}$ alloy. The microstructure of the alloy led to the hierarchical porous structure characterized by larger ligaments (pores) at micron scale (ca. 3–5 μm) and the smaller ligaments (pores) at nanoscale (ca. 50–60 nm) through dealloying. The specific surface areas were up to $47.6 \text{ m}^2 \text{ g}^{-1}$ of HNNPC. The as-prepared HNNPC is a promising electrochemical sensor candidate for glucose due to its excellent electro-catalytic performance. Furthermore, HNNPC can also be a host of other active materials in view of its large specific surface area, free

standing, and exquisite hierarchical nested-network porous structure.

Acknowledgments

We thank the financial support by the “thousands talents” program for the pioneer researcher and his innovation team, China, and the funding support of the National Natural Science Foundation of China (NSFC No. 11572051 and 51501011).

References

- [1] C. Tang, B.Q. Li, Q. Zhang, L. Zhu, H.F. Wang, J.L. Shi, F. Wei, CaO-templated growth of hierarchical porous graphene for high-power lithium-sulfur battery applications, *Adv. Funct. Mater.* 26 (2016) 577–585.
- [2] Z.Y. Xiong, C.L. Liao, W.H. Han, X.G. Wang, Mechanically tough large-area hierarchical porous graphene films for high-performance Flexible supercapacitor applications, *Adv. Mater.* 27 (2015) 4469–4475.
- [3] L.H. Chen, X.Y. Li, G. Tian, Y. Li, J.C. Rooke, G.S. Zhu, S.L. Qiu, X.Y. Yang, B.L. Su, Highly stable and reusable multimodal zeolite TS-1 based catalysts with hierarchically interconnected three-level micro-meso-macroporous structure, *Angew. Chem. Int. Ed.* 50 (2011) 11156–11161.
- [4] K. Tian, X.-X. Wang, H.-Y. Li, R. Nadimicherla, X. Guo, Lotus pollen derived 3-dimensional hierarchically porous NiO microspheres for NO₂ gas sensing, *Sens. Actuators B* 227 (2016) 554–560.
- [5] D. Xie, L. Chang, F. Wang, G. Du, B. Xu, Ultrasound-assisted synthesis of macro/mesoporous ZnO double-pyramids and their optical and photocatalytic properties, *J. Alloys Compd.* 545 (2012) 176–181.
- [6] M. Yao, Z. Hu, Z. Xu, Y. Liu, Template synthesis of 1D hierarchical hollow Co₃O₄ nanotubes as high performance supercapacitor materials, *J. Alloys Compd.* 644 (2015) 721–728.
- [7] J. Wu, L. Zuo, Y. Song, Y. Chen, R. Zhou, S. Chen, L. Wang, Preparation of biomass-derived hierarchically porous carbon/Co₃O₄ nanocomposites as anode materials for lithium-ion batteries, *J. Alloys Compd.* 656 (2016) 745–752.
- [8] Y. Ding, M.W. Chen, Nanoporous metals for catalytic and optical applications, *MRS Bull.* 34 (2009) 569–576.
- [9] D.Y. Zhao, D.W. Fan, J.P. Wang, C.X. Xu, Hierarchical nanoporous platinum-copper alloy for simultaneous electrochemical determination of ascorbic acid, dopamine, and uric acid, *Microchim. Acta* 182 (2015) 1345–1352.
- [10] M.N. Lee, M.A. Santiago-Cordoba, C.E. Hamilton, N.K. Subbaiyan, J.G. Duque, K.A.D. Obrey, Developing monolithic nanoporous gold with hierarchical bicontinuity using colloidal Bijels, *J. Phys. Chem. Lett.* 5 (2014) 809–812.
- [11] J. Erlebacher, M.J. Aziz, A. Karma, N. Dimitrov, K. Sieradzki, Evolution of nanoporosity in dealloying, *Nature* 410 (2001) 450–453.
- [12] Z. Qi, J. Weissmuller, Hierarchical nested-network nanostructure by dealloying, *Acs Nano* 7 (2013) 5948–5954.
- [13] Y. Ding, J. Erlebacher, Nanoporous metals with controlled multimodal pore size distribution, *J. Am. Chem. Soc.* 125 (2003) 7772–7773.
- [14] Z. Qi, U. Vainio, A. Kornowski, M. Ritter, H. Weller, H.J. Jin, J. Weissmuller, Porous Gold with a nested-network architecture and ultrafine structure, *Adv. Funct. Mater.* 25 (2015) 2530–2536.
- [15] J.M. Won, J.H. Kim, Y.J. Choi, J.S. Cho, Y.C. Kang, Electrochemical properties of CuO hollow nanopowders prepared from formless Cu-C composite via nanoscale Kirkendall diffusion process, *J. Alloys Compd.* 671 (2016) 74–83.
- [16] M. Luo, A. Ruditskiy, H.C. Peng, J. Tao, L. Figueroa-Cosme, Z.K. He, Y.N. Xia, Penta-twinned copper nanorods: facile synthesis via seed-mediated growth and their tunable plasmonic properties, *Adv. Funct. Mater.* 26 (2016) 1209–1216.
- [17] H.J. Yang, S.Y. He, H.L. Chen, H.Y. Tuan, Monodisperse copper nanocubes: synthesis, self-assembly, and large-area dense-packed films, *Chem. Mater* 26 (2014) 1785–1793.
- [18] C.Q. Zhang, J.P. Tu, X.H. Huang, Y.F. Yuan, X.T. Chen, F. Mao, Preparation and electrochemical performances of cubic shape Cu₂O as anode material for lithium ion batteries, *J. Alloys Compd.* 441 (2007) 52–56.
- [19] S. Han, S. Hong, J. Yeo, D. Kim, B. Kang, M.Y. Yang, S.H. Ko, Nanorecycling: monolithic integration of copper and copper oxide nanowire network electrode through selective reversible photothermochemical reduction, *Adv. Mater* 27 (2015) 6397–6403.
- [20] M. Srivastava, J. Singh, R.K. Mishra, A.K. Ojha, Electro-optical and magnetic properties of monodispersed colloidal Cu₂O nanoparticles, *J. Alloys Compd.* 555 (2013) 123–130.
- [21] X.Z. Wang, M.J. Chen, Y.R. He, J.Q. Zhu, Shape-controlled preparation of Cu₂O crystals and their growth mechanism, *J. Alloys Compd.* 628 (2015) 50–56.
- [22] W.B. Liu, L. Chen, J.Z. Yan, N. Li, S.Q. Shi, S.C. Zhang, Dealloying solution dependence of fabrication, microstructure and porosity of hierarchical structured nanoporous copper ribbons, *Corros. Sci.* 94 (2015) 114–121.
- [23] W.B. Liu, C.L. Xin, L. Chen, J.Z. Yan, N. Li, S.Q. Shi, S.C. Zhang, A facile one-pot dealloying strategy to synthesize monolithic asymmetry-patterned nanoporous copper ribbons with tunable microstructure and nanoporosity, *RSC Adv.* 6 (2016) 2662–2670.
- [24] J. Li, H.W. Jiang, N.N. Yu, C.X. Xu, H.R. Geng, Fabrication and characterization of bulk nanoporous copper by dealloying Al-Cu alloy slices, *Corros. Sci.* 90 (2015) 216–222.
- [25] W.B. Liu, S.C. Zhang, N. Li, J.W. Zheng, Y.L. Xing, A facile one-pot route to fabricate nanoporous copper with controlled hierarchical pore size distributions through chemical dealloying of Al-Cu alloy in an alkaline solution, *Microporous Mesoporous Mater* 138 (2011) 1–7.
- [26] Q.Q. Kong, L.X. Lian, Y. Liu, J. Zhang, Fabrication and compression properties of bulk hierarchical nanoporous copper with fine ligament, *Mater. Lett.* 127 (2014) 59–62.
- [27] Z. Qi, C.C. Zhao, X.G. Wang, J.K. Lin, W. Shao, Z.H. Zhang, X.F. Bian, Formation and characterization of monolithic nanoporous copper by chemical dealloying of Al-Cu alloys, *J. Phys. Chem. C* 113 (2009) 6694–6698.
- [28] C.C. Zhao, X.G. Wang, Z. Qi, H. Ji, Z.H. Zhang, On the electrochemical dealloying of Mg-Cu alloys in a NaCl aqueous solution, *Corros. Sci.* 52 (2010) 3962–3972.
- [29] Q. Zhang, Z.H. Zhang, On the electrochemical dealloying of Al-based alloys in a NaCl aqueous solution, *Phys. Chem. Chem. Phys.* 12 (2010) 1453–1472.
- [30] T. Song, M. Yan, Z. Shi, A. Atrens, M. Qian, Creation of bimodal porous copper materials by an annealing-electrochemical dealloying approach, *Electrochim. Acta* 164 (2015) 288–296.
- [31] M.Z. Luo, R.P. Baldwin, Characterization of carbohydrate oxidation at copper electrodes, *J. Electroanal. Chem.* 387 (1995) 87–94.
- [32] Y.C. Zhang, L. Su, D. Manuzzi, H.V.E. de los Monteros, W.Z. Jia, D.Q. Huo, C.J. Hou, Y. Lei, Ultrasensitive and selective non-enzymatic glucose detection using copper nanowires, *Biosens. Bioelectron.* 31 (2012) 426–432.
- [33] Y. Zhang, Y. Liu, L. Su, Z. Zhang, D. Huo, C. Hou, Y. Lei, CuO nanowires based sensitive and selective non-enzymatic glucose detection, *Sens. Actuators B* 191 (2014) 86–93.
- [34] G.Y. Liu, B.Z. Zheng, Y.S. Jiang, Y.Q. Cai, J. Du, H.Y. Yuan, D. Xiao, Improvement of sensitive CuO NFs-ITO nonenzymatic glucose sensor based on in situ electrospun fiber, *Talanta* 101 (2012) 24–31.
- [35] E. Reitz, W.Z. Jia, M. Gentile, Y. Wang, Y. Lei, CuO nanospheres based nonenzymatic glucose sensor, *Electroanalysis* 20 (2008) 2482–2486.
- [36] S. Park, H. Boo, T.D. Chung, Electrochemical non-enzymatic glucose sensors, *Anal. Chim. Acta* 556 (2006) 46–57.
- [37] K.E. Toghill, R.G. Compton, Electrochemical non-enzymatic glucose sensors: a perspective and an evaluation, *Int. J. Electrochem. Sci.* 5 (2010) 1246–1301.
- [38] Z.N. Liu, B.L. Yadian, H. Liu, C. Liu, B.W. Zhang, R.V. Ramanujan, Y.Z. Huang, Fabrication of hybrid CuO/Pt/Si nanoarray for non-enzymatic glucose sensing, *Electrochem. Commun.* 33 (2013) 138–141.
- [39] R.K. Shervedani, A.H. Mehrjardi, N. Zamiri, A novel method for glucose determination based on electrochemical impedance spectroscopy using glucose oxidase self-assembled biosensor, *Bioelectrochem* 69 (2006) 201–208.